Peer-reviewed version available at Sensors 2018, 19, 91; doi:10.3390/s19010091

A facile and high selectivity novel fluorescence sensing determination of 2, 4, 6-trinitrophenol based on cationic water-soluble pillar[6]arene graphene nanocomposite

Xiaoping Tan*, Tingying Zhang, Wenjie Zeng, Shuhua He, Xi Liu, Hexiang Tian, Jianwei Shi, Tuanwu Cao*

Key Lab of Inorganic Special Functional Materials, Chongqing Municipal Education Commission, School of Chemistry and Chemical Engineering, Yangtze Normal University, Chongqing, 408100, China

***Corresponding Author**

E-mail: xptan@yznu.cn (X. Tan); caotuanwu@yznu.cn (T. Cao)

Abstract: We describe a selective and sensitive fluorescence platform for the detection of trinitrophenol (TNP) based on competitive host–guest recognition between pyridine-functionalized pillar[6]arene (PCP6) and probe (acridine orange, AO) that used PCP6-functionalized reduced graphene (PCP6-rGO) as the receptor. TNP is an electron-deficient and negative molecule which is captured by PCP6 via electrostatic interactions and π-π interactions. Therefore, a selective and sensitive fluorescence sensor for TNP detection is developed. It has a low detection limit of 0.0035 μM (S/N=3) and a wider linear response of 0.01−5.0 and 5.0−125.0 for TNP. The sensing platform is also used to test TNP in two water and soil samples with satisfying results. This suggests that this approach has potential applications for the determination of TNP.

Keywords: cationic pillar[6]arene, host–guest recognition, reduced graphene, trinitrophenol

1. Introduction

Nitroaromatics (NACs) are toxic and explosive.[1,2] Nitroaromatic explosives are common components of industrial explosives, such as 2,4,6-trinitrophenol (TNP), 2,4-dinitrotoluene (DNT), and 2,4,6-trinitromethylbenzene (TNT).[3] TNP is more explosive than TNT, and it has been widely used in the military as well as in objects that include fireworks, dyes and glasses.[4] TNP might harm the skin and eyes and can damage organs. It is an environmental pollutant and harmful to human health. Therefore, rapid, selective and sensitive determination of TNP is increasingly important for security and environmental protection.

TNP is currently determined by using solid-phase microextraction,[5,6] spectrophotometry,[7] X-ray imaging,[8] gas chromatography (GC),[9] capillary electrophoresis (CE),[10] high-performance liquid chromatography (HPLC),[11] and electrochemical methods.[12,13] Unfortunately, these methods often need a complicated synthetic process or labeling procedure—these are time consuming, expensive and complicated. In recent years, fluorescence techniques have been shown

Peer-reviewed version available at Sensors 2018, 19, 91; doi:10.3390/s19010091

to be a promising method for the detection of TNP. They exhibit many advantages over other common detection techniques: they are low cost, sensitive, selective and portable.[14]

For example, Rong et al.[15] developed a label-free fluorescence sensing method that used chemically oxidized and liquid exfoliated g-C_3N_4 nanosheets for the determination of TNP with a detection limit of 8.2×10^{-6} M. Ma et al.[16] prepared dual-emissive electropolymerization films as fluorescent sensors for the detection of TNT. Peng et al.[17] constructed a new BNQD-based turn-off sensor for the sensitive detection of TNP based on the strong IFE between TNP and the BNQDs—the linear range was $2.5 \times 10^{-7} – 2.0 \times 10^{-4}$ M and the detection limit was 1.4×10^{-7} M.

Many fluorescent probes have been prepared for TNP determination including the graphitic carbon nitride (g-C_3N_4) nanosheets,[15-17] metal-organic frameworks,[18-22] transition-metal dichalcogenide nanostructures,[23,24] graphene quantum dots (GQDs),[25-27] conjugated polymers (CPs),[28] and other carbon-based nanomaterials.[29-34] Although many fluorescence sensing probes have been reported, none are suitably fast, sensitive and selective. Therefore, tools for selective and sensitive detection of TNP are still an unmet need.

Macrocyclic arenes have been widely studied in the field of supramolecular chemistry.[35-37] After crown ethers, calixarenes, cyclodextrins, and cucurbiturils,[38,39] pillar[n]arenes are the fifth class of macrocyclic host molecules, and they are firstly reported by Ogoshi.[40] Pillar[n]arenes mainly consist of pillar[5]arenes and pillar[6]arenes, which are linked by methylene bridges at their *para*-positions to form a unique rigid pillar architecture. Pillar[n]arenes are important players in supramolecular chemistry because of them easy synthesis, unique pillar shape, symmetrical structure, versatile functionalization, excellent host-guest properties, and natural supramolecular assembly characteristics. They have been widely applied in host-guest chemistry and biomedical material.[41-45] However, by comparing other conventional macrocyclic hosts, their application in sensor is rare.

Recently, Shao et al.[46] reported a novel fluorescent supramolecular cross-linked polymer network that could detect TNP in solutions and films via pillar[5]arene-based

host-guest recognition. The combination of supramolecular chemistry and conjugated polymer science as well as the co-constructed supramolecular network system can pave the way for new multi-functional fluorescent materials. The using of a water-soluble macrocyclic host that interacts with graphene by π–π stacking can improve selectivity and sensitivity.[47-50] Graphene has unique thermal, electronic and mechanical properties as well as a high surface area, low cost, and low toxicity due to its strictly 2D structure.[51] It has been applied in sensing, drug carriers and other technological fields.

While host-guest recognition has potential applications in many areas, including sensors, gene and drug delivery, nanoelectronics, and supramolecular polymers, high recognition and binding strength. The guest TNP is an electron-deficient molecule and is easily captured by the electron-rich cavity of the cationic pillar[6]arene. Therefore, we describe a competitive fluorescence sensing platform based on pyridine-functionalized pillar[6]arene and reduced graphene PCP6-rGO nanocomposite for determination TNP. The PCP6 is grafted on the surface of rGO via π–π stacking to obtain the receptor. The indicator/dye molecule AO is first bound to the receptor. A competitive analyte is then added to the sensing ensemble leading to recovery AO fluorescence via indicator displacement. Therefore, TNP can be successfully determined by a competitive fluorescence method based on a host-guest competitive recognition. The competitive fluorescence sensing platform based on PCP6-rGO is illustrated in **Fig. 1**. This method is simple, low cost, sensitive, selective and has been successfully applied to TNP detection in tap water, lake water and soil samples.

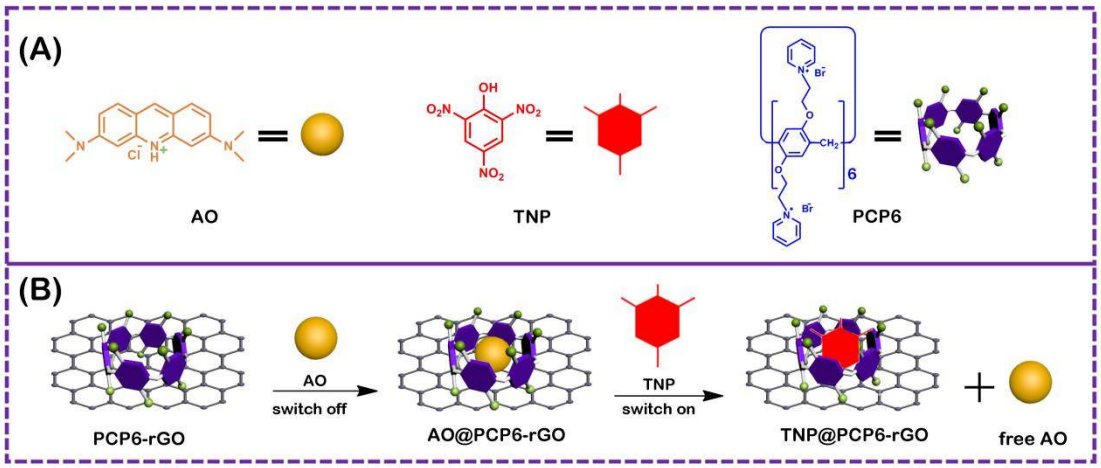

Figure 1. The corresponding cartoon representations of AO, TNP and PCP6 (A), and the illustration of PCP6-rGO nanohybrids-based fluorescent sensing method towards trinitrophenol (B).

2. Experimental

2.1. Reagents

Graphene oxide (GO) was obtained from Nanjing XFNANO Materials Tech Co., Ltd. (Nanjing, China). Acridine orange (AO) and trinitrophenol (TNP) were acquired from Sigma Chemical Co. (St. Louis, MO, USA). PCP6 was synthesized according to the literature,[52-54] and the synthetic route is shown in **Scheme S1.** The structure and purity of all compounds were confirmed by ^{1}H NMR and ^{13}C NMR (see **Figs. S1–S8)**. Detailed synthetic procedures and analytical data are given in the Supporting Information (SI). Other chemicals were of analytical grade. Deionized water (DW, 18 MΩ cm) was used to prepare all of the aqueous solutions.

2.2. Apparatus and instruments

The samples are characterized by Fourier transform infrared (FTIR) spectroscopy via the SCIENTIFIC Nicolet IS10 (Massachusetts, New York, USA) FTIR impact 410 spectrophotometer using KBr pellets at a wavelength of 4000–400 cm^{-1}. Thermogravimetric analysis (TGA) at 25 to 800°C with a heating rate of 10°C min^{-1} in nitrogen is performed in the Q50 TGA (TA Instruments, New Castle, USA). The X-ray photoelectron spectroscopy (XPS) is performed on an ESCALAB-MKII

spectrometer (VG Co., London, United Kingdom) with Al Ka X-ray radiation as the X-ray source for excitation. The zeta potential of the sample is measured with a Malvern Zetasizer Nano series. Fluorescent titrimetric experiments are performed on a Hitachi F-4500 spectrophotometer (Tokyo, Japan).

2.3. Synthesis of the PCP6-rGO hybrid materials

The PCP6-rGO composite was synthesized by heating and stirring the GO suspension under strong alkaline conditions in the presence of sodium citrate and PCP6.[55-57] The GO (20 mg) was dispersed in a solution of PCP6 (20 mg) and sodium citrate (100mg) in DW (50 mL) by sonication, and the pH of mixtures was adjusted to 12 by NaOH solution (1 M); the mixtures were then stirred at 90°C for 5 h. The black dispersion of PCP6-rGO was separated by centrifuging with 13000 rpm for 1 h and washed with DW three times to obtain PCP6-rGO composite. A control experiment for the prepared rGO was developed in absence of PCP6 solution, and the PCP6-rGO was stable for over six months; photographs of PCP6-rGO and rGO aqueous dispersion were shown in **Fig. S9**.

2.4. Fluorescent experiments

Aqueous solutions of AO (100 μM), TNP (200 μM), and PCP6-rGO (1.0 mg mL^{-1}) were prepared by DW, respectively. A final concentration of 10 μM AO was also obtained via dilution. PCP6-rGO was gradually added to the AO solution, and the fluorescence of the AO was gradually quenched. The competitive displacement experiments were as follows: the TNP solution was gradually added into complex of AO@bound PCP6-rGO to displace the AO molecule from the cavity of PCP6. The fluorescence signal was measured and recorded after the combined solution was mixed by vortexing for 3 min.

3. Results and Discussion

3.1. Characterization of the PCP6-rGO hybrid nanomaterial

The GO and PCP6-rGO are characterized by UV-vis spectroscopy (**Fig. 2)**. The UV-vis spectroscopy of GO dispersion shows strong adsorption at ~230 nm and the peak gradually red-shifts from 230 to 260 nm (PCP6-rGO), suggesting that GO is reduced to rGO by sodium citrate under strong alkaline conditions.[58-61] We further characterize the microstructure of PCP6-rGO by TEM (**Fig. 2B**). The TEM image reveals that PCP6-rGO material is randomly aggregated thin, wrinkled sheets closely associated with each other. And it is difficult to distinguish the PCP6 on the surface of rGO, therefore, the PCP6-rGO is further characterized by FTIR, zeta, TGA, and XPS. The FTIR spectrums of rGO, PCP6-rGO, and PCP6 are shown in **Fig. 3A**. Firstly, The FTIR of rGO shows some weak adsorptions due to a small amount of the remaining oxygen-containing functional groups.[47] Secondly, the FTIR spectrum of PCP6-rGO and PCP6 are very similar. The bands located at 1590 cm^{-1}, 1556 cm^{-1}, and 1409 cm^{-1} are ascribed to the phenyl in PCP6. The bands at 1618 cm^{-1} and 1388 cm^{-1} are attributed to pyridine of PCP6. The FTIR results indicate that PCP6 has grafted on the surface of rGO and forms the PCP6-rGO composite. The PCP6-rGO is also characterized by the TGA (**Fig. 3B)**. The mass loss of rGO is only 6 wt% at 600 °C due to the decomposition of remaining oxygen-containing functional groups. The mass loss of the PCP6-rGO reaches approximately 56 wt % when the temperature is 550 °C. Thus, the mass loss caused by decomposition of PCP6 is to be 50.0 wt % when the mass loss of rGO is deducted. The zeta potential measurements of PCP6-rGO and rGO are obtained and demonstrated in **Fig. 3C**. The zeta potential of PCP6-rGO is 35 mV, the increased zeta potential value is attributed to the large number of positive charged pyridinium units in the PCP6 molecule. Moreover, the PCP6-rGO zeta potential is higher than 30 mV,[62] indicating that the stability and dispersion of PCP6-rGO are very high.

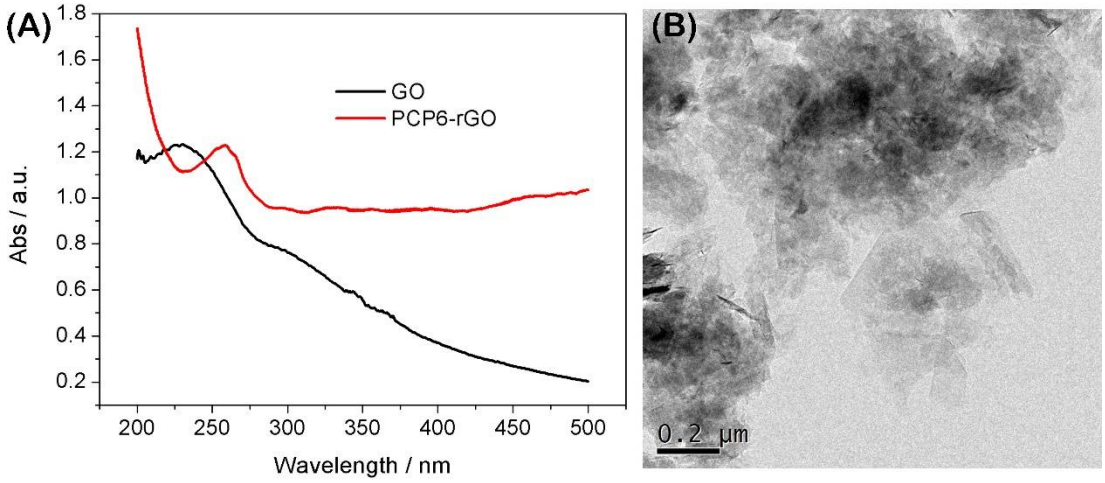

Figure 2. UV-vis spectra of the GO and PCP6-rGO in aqueous solution (A); TEM image of PCP6-rGO.

The XPS results of rGO and PCP6-rGO are provided in **Fig. 3D**. A significant N 1s peak is observed in the PCP6-rGO samples, but no N signal is detected on the rGO film, showing that rGO has been functionalized by PCP6. In addition, the intensities of C=C/C–C peaks in PCP6-rGO predominated upon comparing the C 1s of GO. **Figs. 3E** and **3F** show that the intensities of all of the C 1s peaks of C–O, C=O, and O–C=O obviously decrease indicating that the GO is reduced to rGO. Therefore, above aforementioned results of FTIR, TGA, zeta potential, and XPS suggest that PCP6 has successfully self-assembled on the surface of rGO by π–π interaction between rGO and PCP6.[63,64]

Preprints (www.preprints.org) | NOT PEER-REVIEWED | Posted: 28 November 2018 doi:10.20944/preprints201811.0605.v1

Peer-reviewed version available at Sensors 2018, 19, 91; doi:10.3390/s19010091

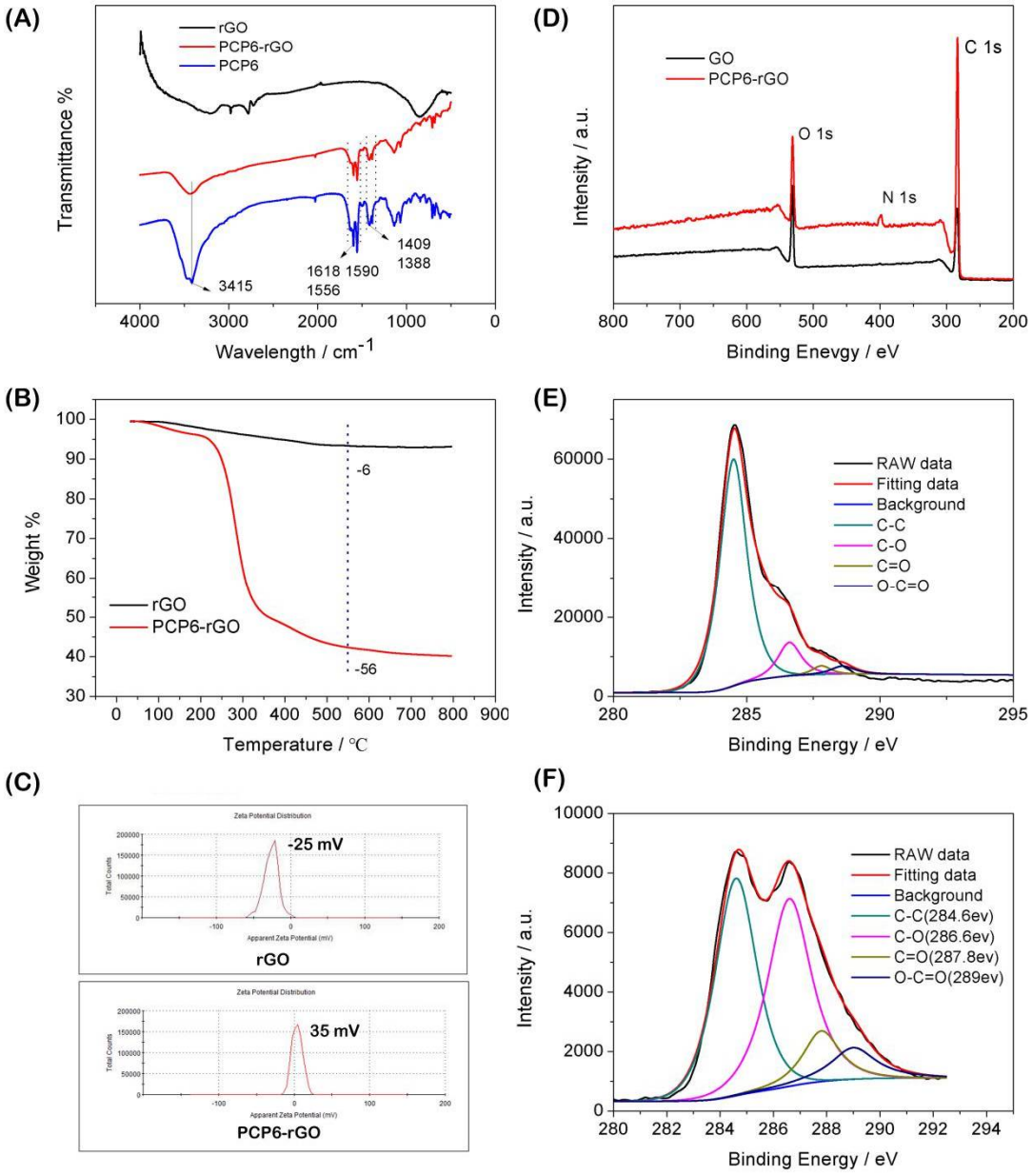

Figure 3. FTIR spectra of rGO, PCP6-rGO and PCP6 (A). TGA curves of rGO, and PCP6-rGO (B). Zeta potentials of rGO and PCP6-rGO (C). XPS survey spectra of GO and PCP6-rGO (D). The C1s XPS spectra of GO (E) and PCP6-rGO (F).

3.2. Fluorescence spectra analysis

We first study the fluorescence quenching ability of PCP6 and PCP6-rGO towards AO. While the fluorescence intensity of AO decreases with PCP6 via host-guest recognition interactions (**Fig. S10**), the fluorescence intensity of AO quenching is mainly due to PCP6-rGO based on the outstanding fluorescent quenching

performance of rGO. The fluorescence quenching of the dye is caused by the fluorescence resonance energy transfer (FRET) between dye and graphene.[50,55,57] The host-guest between PCP6 and AO is studied by UV-vis and shown in **Fig. S11**. The AO exhibits an absorption at 490 nm, and the absorption intensity gradually decreases with the increasing of PCP6, and a new absorption is observed at 503 nm, then the red shift occurred. This results are accordance with the reported work by Hua and co-workers.[65]

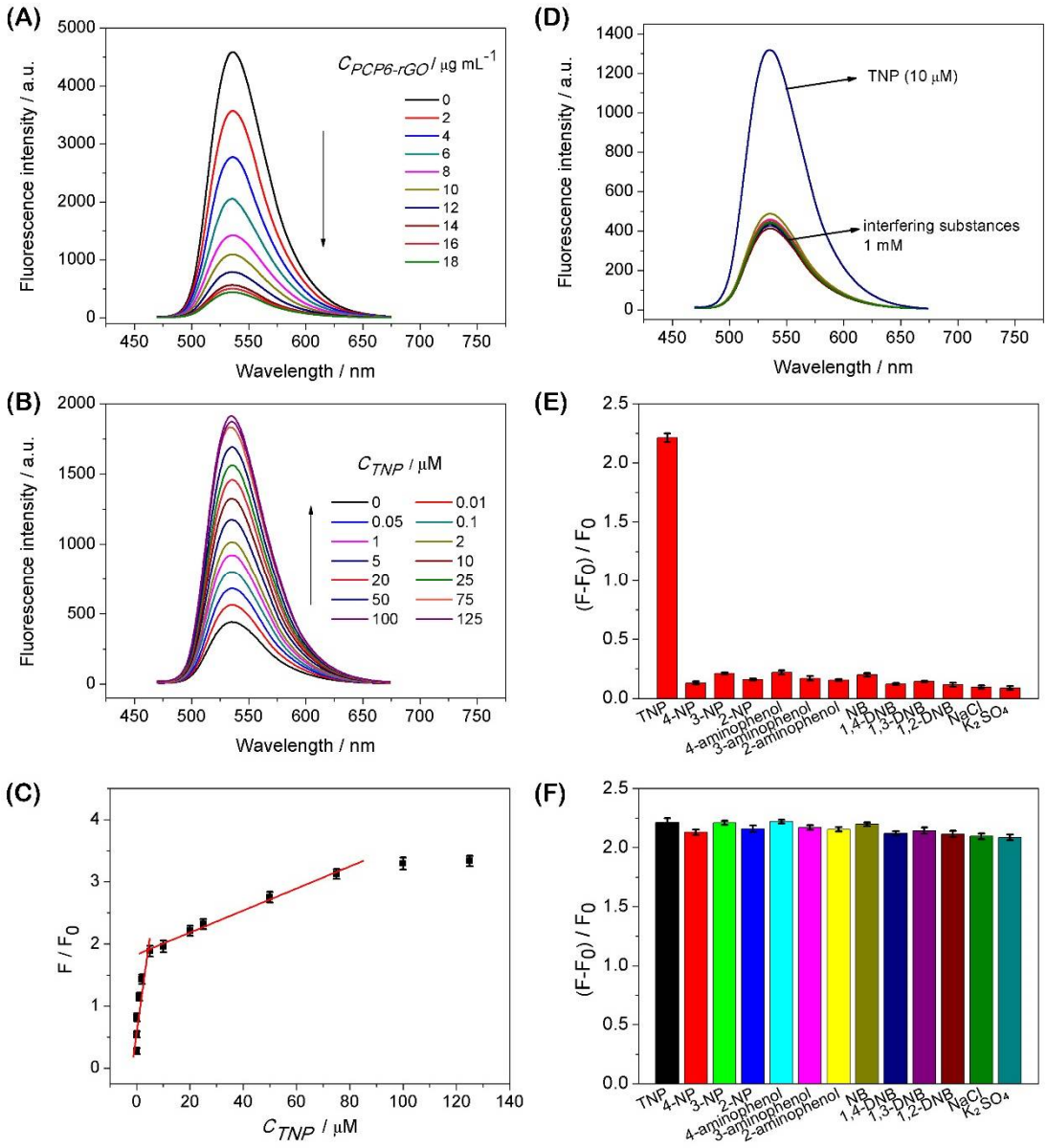

Figure 4. The effect of increasing concentrations of PCP6-rGO (concentrations ranging from 0 μg/mL to 18 μg/mL) on the fluorescence intensity of AO (λex = 460 nm) dispersion (A). Fluorescence spectra of the AO@PCP6-rGO complexes via

Peer-reviewed version available at Sensors 2018, 19, 91; doi:10.3390/s19010091

different concentrations of TNP (B). Calibration curves of fluorescent intensity for AO@PCP6-rGO *vs*. TNP concentrations (C). Fluorescent spectra of AO@PCP6-rGO in the presence of TNP and others interferences (D). The relative fluorescence intensity of $(F-F_0)/F_0$, and the F_0 and F are the fluorescence intensity without and with the presence of 10 μM TNP and 1mM interferences (E). The relative fluorescence intensity $[(F-F_0)/F_0]$ of 10 μM TNP in the absence 1mM others interferences (F).

Fig. 4A shows the fluorescence quenching performance with PCP6-rGO towards AO. The fluorescence of AO is continuously quenched with increasing PCP6-rGO. **Fig. 4B** shows the successive reversal of the AO fluorescence signal with repeated TNP dosing on the pre-formed AO@PCP6-rGO inclusion. The fluorescence signal reversion is caused by the addition of TNP amount, which suggests the successful detection of TNP via this fluorescence approach. Therefore, we conclude that AO enteres into the cavity of PCP6 and formed an inclusion complex with PCP6-rGO.

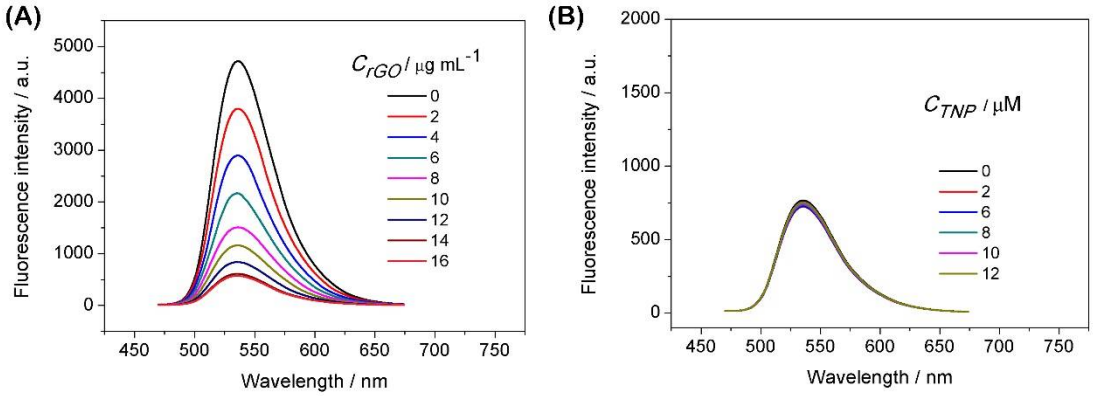

Figure 5. (A) The effect of increasing concentrations of rGO (concentrations ranging from 0 to 16 μg mL^{-1}) on the fluorescence intensity of 10 μM AO (λex = 460 nm). (B) Fluorescence spectra of the AO@rGO complex via different concentrations of TNP.

Fig. S12 shows that the fluorescence of AO is recovered by the TNP (20 μM), and the effects are similar at 25 °C, 35 °C, 45 °C and 50 °C, indicating that the changes in temperature does not affect the sensing performance. In addition, the AO is released from the cavity of PCP6 by addition of TNP based on the competitive supramolecular recognition. This is a "switch-off-on" fluorescence process. The AO

is also incubated with PCP6-rGO to form an AO@PCP6-rGO complex that is attached to the rGO. This is accompanied by indicator fluorescence 'turn off' due to FRET.[50,55,57] Some control experiments are performed to confirm that the observed fluorescent intensity recovery is caused by the displacement of AO by TNP from the cavity of PCP6 host molecule. Although **Figs. 5A** and **5B** show that the fluorescence quenching phenomenon obviously occurs between rGO and AO, the fluorescence reversion does not recover upon addition of TNP. Therefore, the dye indicator AO first combines with PCP6-rGO and is then released from the cavity of PCP6 upon the addition of TNP. This forms a fluorescent switch.

Fig. 4C presentes the calibration curves for the quantitative determination of TNP, and the fluorescence ratio F/F_0 is proportional to the concentration of TNP. The linear response ranges for TNP detection are 0.01−5.0 and 5.0−125.0 μM. The detection limit is 0.0035 μM (S/N=3), and the corresponding regression equations of F/F_0=0.26 C (μM) + 0.65 and F/F_0=0.02 C (μM) + 1.84 are also obtained. This approach is compared to other methods for detection of TNP (**Table S1)**. This competitive fluorescent method shows a wider linear range, lower detection limit, and high selectivity versus previously reported approaches. Moreover, this method is very convenient and simple for the determination of TNP.

3.3. The analysis of host–guest recognition

The three nitro groups are strong electron-withdrawing groups, thus the trinitrophenol is an electron-deficient molecule. It is easily captured by electron-rich cavity of the pillararenes.[66-68] The nitro moiety on TNP makes it quite negative, and the molecular size of TNP is suitable for the PCP6 cavity that is captured by the positively charged pillar[6]arene via the electrostatic interactions that plays an important role in host-guest recognition.[65] Therefore, the TNP molecule can be easily recognized by cationic and electron-rich PCP6—this leads to the high selectivity for TNP detection.

3.4. Selectivity and practical samples analysis

The interference study for detection of TNP with AO-bound PCP6-rGO are measured with 100-fold concentrations of TNP analogues (4-NP, 3-NP, 2-NP, 4-aminophenol, 3-aminophenol, 2-aminophenol, NB, 1,4-DNB, 1,3-DNB and 1,2-DNB) and common interferents (NaCl and K_2SO_4). The chemical structures of analogues are shown at **Fig. S13**. **Fig. 4D** shows that fluorescence intensity has not change when these interferences are added to AO@PCP6-rGO by comparing TNP in the presence of AO@PCP6-rGO. **Fig. 4E** shows a significant fluorescence increase upon the addition of TNP. However, the addition of other competitive interferents do not caused significant fluorescence changes. In addition, **Fig. 4F** illustrates that the fluorescence intensity of AO has no changes when other competitive interferents are added to a mixture of AO@PCP6-rGO and TNP—this demonstrates that these interferents do not cause a false-positive signal.

To assess AO@PCP6-rGO in practical applications, TNP is detected with standard addition method in two water samples and a soil sample. The procedure of preparing practical samples is elaborated as follows: Soil (50 mg) is added to DW (100 mL) under sonication, then the solution is filtrated by filter membrane (0.45 μM) for removing insoluble solid matter. The tap and lake water samples are collected at tap water and lake water. The practical detection TNP is carried out by standard addition methods in prepared soil sample. The procedure of detection TNP in water samples is similar with soil sample. The recoveries are 98.5-101.4%, and the RSDs are 1.7–5.8% in **Table 1**. The accuracy and precision of this proposed approach are satisfactory, which indicate that the proposed method can be applied for the detection of TNP in water and soil samples.

Table 1 Determination of TNP in tap water, lake water and soil samples.

Sample	Added (μM)	Founded (μM)	RSD (%)	Recovery (%)
Tap water	0	0	-	-
	2	1.95 ± 0.06	3.1	97.5
	5	5.07 ± 0.15	2.9	101.4
	10	9.89 ± 0.32	3.2	98.9
Lake water	0	0	-	-
	2	1.97 ± 0.11	5.5	98.5
	5	4.97 ± 0.09	1.8	99.4
	10	10.09 ± 0.21	2.1	100.9
Soil	0	0	-	-
	2	2.06 ± 0.12	5.8	103
	5	4.97 ± 0.19	3.8	99.4
	10	9.95 ± 0.17	1.7	99.5

4. Conclusions

In conclusion, we describe a simple, convenient, and selective switch-off-on fluorescent sensing platform using pyridine-functionalized water-soluble cationic pillar[6]arene PCP6 and dye acridine orange AO nanocomposite as the energy donor-acceptor. The outstanding host–guest recognition capability of PCP6 and excellent quenching performance of rGO lead to this fluorescent sensing system suitable for TNP detection in tap water, lake water and soil samples. This work demonstrates that the PCP6-rGO composite is a good energy acceptor for fluorescence sensing platforms with potential applications in many fields.

Supporting Information: Synthesis and characterization of PCP6 host molecule; the structures of TNP and other interference molecules; the comparison of some reported methods with the present fluorescence approach for determination of TNP; and others information.

Acknowledgements: This work was financially supported by the Program for Leading Talents, the Basic Research Project of Science and Technology Commission of Chongqing (Grant No. cstc2017jcyjAX0031), the Education Commission of Chongqing (Grant No. KJ1712298), the Research Foundations of Yangtze Normal

University (2015XJXM02, 2016XJQN26) and School Enterprise Innovation Platform (Grant No. FLKW2017AAA1024). We would like to thank LetPub (www.letpub.com) for providing linguistic assistance during the preparation of this manuscript.

Conflicts of Interest: The authors declare no conflict of interest.

References

1. Salinas, Y.; Martinez-Manez, R.; Marcos, M.D.; Sancenon, F.; Costero, A.M.; Parra, M.; Gil, S. Optical chemosensors and reagents to detect explosives. *Chem. Soc. Rev*. **2012**, *41*, 1261−1296.
2. Germain, M.E.; Knapp, M.J. Optical explosives detection: from color changes to fluorescence turn-on. *Chem. Soc. Rev*. **2009**, *38*, 2543−2555.
3. Ma, Y.; Huang, S.; Deng, M.; Wang, L. White upconversion luminescence nanocrystals for the simultaneous and selective detection of 2,4,6-trinitrotoluene and 2,4,6-trinitrophenol. *ACS Appl. Mater. Interfaces* **2014**, *6*, 7790−7796.
4. Han, Y.; Chen, Y.; Feng, J.; Liu, J.; Ma, S.; Chen, X. One-pot synthesis of fluorescent silicon nanoparticles for sensitive and selective determination of 2,4,6-trinitrophenol in aqueous solution. *Anal. Chem*. **2017**, *89*, 3001−3008.
5. Berg, M.; Bolotin, J.; Hofstetter, T.B. Compound-specific nitrogen and carbon isotope analysis of nitroaromatic compounds in aqueous samples using solid-phase microextraction coupled to GC/IRMS. *Anal. Chem*. **2007**, *79*, 2386−2393.
6. Guerra-Diaz, P.; Gura, S.; Almirall, J.R. Dynamic planar solid phase microextraction−ion mobility spectrometry for rapid field air sampling and analysis of illicit drugs and explosives. *Anal. Chem*. **2010**, *82*, 2826−2835.
7. Uzer, A.; Ercag, E.; Apak, R. Selective spectrophotometric determination of trinitrotoluene, trinitrophenol, dinitrophenol and mononitrophenol. *Anal. Chim. Acta*. **2004**, *505*, 83–93.
8. Luggar, R.; Farquharson, M.; Horrocks, J.; Lacey, R. Multivariate analysis of statistically poor EDXRD spectra for the detection of concealed explosives. *X-ray Spectrom*. **1998**, *27*, 87-94.
9. Tesarova, E.; Sykora, D.; Voznakova, Z. GC and HPLC determination of nitrophenol related pesticides. *Fresen. Environ. Bull*. **1995**, *4*, 609–616.

10. Zhang, H.Y.; Wang, M.; Zhao, J.Y.; Shi, Z.H. Sandwich-type spontaneous injection of nitrophenols for capillary electrophoresis analysis. *Anal. Meth*. **2012**, *4*, 2177–2182.

11. Yamauchi, Y.; Ido, M.; Ohta, M.; Maeda, H. High performance liquid chromatography with an electrochemical detector in the cathodic mode as a tool for the determination of p-nitrophenol and assay of acid phosphatase in urine samples. *Chem. Pharm. Bull*. **2004**, *52*, 552–555.

12. Forzani, E.S.; Lu, D.; Leright, M.J.; Aguilar, A.D.; Tsow, F.; Iglesias, R.A.; Zhang, Q.; Lu, J.; Li, J.; Tao, N. A hybrid electrochemical-colorimetric sensing platform for detection of explosives. *J. Am. Chem. Soc*. **2009**, *131*, 1390–1391.

13. Yan, F.; He, Y.Y.; Ding, L. H.; Su, B. Highly ordered binary assembly of silica mesochannels and surfactant micelles for extraction and electrochemical analysis of trace nitroaromatic explosives and pesticides. *Anal. Chem*. **2015**, *87*, 4436–4441.

14. Xu, S.F.; Lu, H.Z. Ratiometric fluorescence and mesoporous structure dual signal amplification for sensitive and selective detection of TNT based on MIP@QD fluorescence sensors. *Chem. Commun*. 2015, **51**, 3200–3203.

15. Rong, M.C.; Lin, L.P.; Song, X.H.; Zhao, T.T.; Zhong, Y.X.; Yan, J.W.; Wang, Y.R.; Chen, X. A label-free fluorescence sensing approach for selective and sensitive detection of 2,4,6-trinitrophenol (TNP) in aqueous solution using graphitic carbon nitride nanosheets. *Anal. Chem*. **2015**, *87*, 1288−1296.

16. Ma, H.W.; Li, F.; Yao, L.; Feng, Y.T.; Zhang, Z.X.; Zhang, M. Dual-emissive electropolymerization films for the ratiometric fluorescence detection of TNT and TNP with high sensitivity and selectivity. *Sens. Actuators, B* **2018**, *259*, 380–386.

17. Peng, D.; Zhang, L.; Li, F.F.; Cui, W.R.; Liang, R.P.; Qiu, J.D. Facile and green approach to the synthesis of boron nitride quantum dots for 2,4,6-trinitrophenol sensing. *ACS Appl. Mater. Interfaces* **2018**, *10*, 7315−7323.

18. Cao, L.H.; Shi, F.; Zhang, W.M.; Zang, S.Q.; Mak, T.C.W. Selective sensing of Fe^{3+} and Al^{3+} ions and detection of 2,4,6-trinitrophenol by a water-stable terbium-based metal-organic framework. *Chem. Eur. J*. **2015**, *21*, 15705–15712.

19. Zhang, L.; Kang, Z.; Xin, X.; Sun, D. Metal–organic frameworks based luminescent materials for nitroaromatics sensing. *CrystEngComm*. **2016**, *18*, 193−206.

20. Nagarkar, S.S.; Desai, A.V.; Samanta, P.; Ghosh, S.K. Aqueous phase selective

396 detection of 2,4,6-trinitrophenol using a fluorescent metal–organic framework
397 with a pendant recognition site. *Dalton Trans*. **2015**, *44*, 15175–15180.
398 21. Wang, B.; Lv, X.-L.; Feng, D.; Xie, L.-H.; Zhang, J.; Li, M.; Xie, Y.; Li, J.-R.;
399 Zhou, H.-C. Highly stable Zr(IV)-based metal–organic frameworks for the
400 detection and removal of antibiotics and organic explosives in water. *J. Am. Chem.*
401 *Soc*. **2016**, *138*, 6204−6216.
402 22. Dalapati, S.; Jin, S.; Gao, J.; Xu, Y.; Nagai, A.; Jiang, D. An azine-linked covalent
403 organic framework. *J. Am. Chem. Soc*. **2013**, *135*, 17310−17313.
404 23. Wang, Y.; Ni, Y. Molybdenum disulfide quantum dots as a photoluminescence
405 sensing platform for 2,4,6-trinitrophenol detection. *Anal. Chem*. **2014**, *86*,
406 7463−7470.
407 24. Haldar, D.; Dinda, D.; Saha, S.K. High selectivity in water soluble MoS_2 quantum
408 dots for sensing nitro explosives. *J. Mater. Chem. C* **2016**, *4*, 6321−6326.
409 25. Goldman, E.R.; Medintz, I.L.; Whitley, J.L.; Hayhurst, A.; Clapp, A.R.; Uyeda,
410 H.T.; Deschamps, J.R.; Lassman, M.E.; Mattoussi, H. A hybrid quantum
411 dot−antibody fragment fluorescence resonance energy transfer-based TNT sensor.
412 *J. Am. Chem. Soc*. **2005**, *127*, 6744−6751.
413 26. Wang, Y.; Li, Y.N. Molybdenum disulfide quantum dots as a photoluminescence
414 sensing platform for 2,4,6-trinitrophenol detection. *Anal. Chem*. **2014**, *86*,
415 7463−7470.
416 27. Li, Z.; Wang, Y.; Li, Y.N.; Kokot, S. A sensor based on blue luminescent graphene
417 quantum dots for analysis of a common explosive substance and an industrial
418 intermediate 2,4,6-trinitrophenol. *Spectrochimica Acta Part A: Molecular and*
419 *Biomolecular Spectroscopy* **2015**, *137*, 1213–1221.
420 28. Sang, N.N.; Zhan, C.X.; Cao, D.P. Highly sensitive and selective detection of
421 2,4,6-trinitrophenol using covalent-organic polymer luminescent probes. *J. Mater.*
422 *Chem. A* **2015**, *3*, 92–96.
423 29. Sadhanala, H.K.; Nanda, K.K. Boron and nitrogen Co-doped carbon nanoparticles
424 as photoluminescent probes for selective and sensitive detection of picric acid. *J.*
425 *Phys. Chem. C* **2015**, *119*, 13138−13143.
426 30. Chen, S.; Song, Y.; Shi, F.; Liu, Y.; Ma, Q. Sensitive detection of picric acid based
427 on creatinine-capped solid film assembled by nitrogen-doped graphene quantum
428 dots and chitosan. *Sens. Actuators, B* **2016**, *231*, 634−640.
429 31. Dong, S.J.; Hu, J.S.; Wu, K.; Zheng, M.D. A Mg(II)-MOF as recyclable

luminescent sensor for detecting TNP with high selectivity and sensitivity. *Inorg. Chem. Commun*. **2018**, *95*, 111–116.

32. Ge, L.; Wang, W.X.; Sun, X.M.; Hou, T.; Li, F. Affinity-mediated homogeneous electrochemical aptasensor on graphene platform for ultrasensitive biomolecule detection via exonuclease-assisted target-analog recycling amplification. *Anal. Chem*. **2016**, *88*, 2212–2219.
33. Ma, Y.H.; Zhao, L.; Li, Y.; Liu, J.Y.; Yang, Y.Q.; Chu, T.S. Investigation on sensing mechanism of a fluorescent probe for TNP detection in aqueous solution. *Tetrahedron* **2018**, *74*, 2684–2691.
34. Jigyasa, J.K.R. "ON-OFF" novel fluorescent chemosensors based on nanoaggregates of triaryl imidazoles for superselective detection of nitro-explosive trinitrophenol in multiple solvent systems. *Sens. Actuators B Chem*. **2018**, *259*, 990–1005.
35. Dalgarno, S. J.; Thallapally, P. K.; Barbour, L. J.; Atwood, J. L. Engineering void space in organic van der Waals crystals: calixarenes lead the way. *Chem. Soc. Rev*. **2007**, *36*, 236–245.
36. Gong, H.-Y.; Rambo, B.M.; Karnas, E.; Lynch, V.M.; Sessler, J.L.; Gong, H.-Y.; Rambo, B.M. Rambo. A 'Texas-sized' molecular box that forms an anion-induced supramolecular necklace. *Nat. Chem*. **2010**, *2*, 406–409.
37. Ma, X.; Zhao, Y. Biomedical applications of supramolecular systems based on host–guest interactions. *Chem. Rev*. **2015**, *115*, 7794–7839.
38. Crini, G. Review: A history of cyclodextrins. *Chem. Rev*. **2014**, *114*, 10940–10975.
39. Cragg, P.J.; Sharma, K. Pillar[5]arenes: fascinating cyclophanes with a bright future. *Chem. Soc. Rev*. **2012**, *41*, 597–607.
40. Ogoshi, T.; Kanai, S.; Fujinami, S.; Yamagishi, T.; Nakamoto, Y. para-bridged symmetrical pillar[5]arenes: their lewis acid catalyzed synthesis and host–guest property. *J. Am. Chem. Soc*. **2008**, *130*, 5022–5023.
41. Ogoshi, T.; Yamagishi, T.; Nakamoto, Y. Pillar-shaped macrocyclic hosts pillar[n]arenes: new key players for supramolecular chemistry. *Chem. Rev*. **2016**, *116*, 7937–8002.
42. Strutt, N.L.; Zhang, H.C.; Schneebeli, S.T.; Stoddart, J.F. Functionalizing Pillar[n]arenes. *Acc. Chem. Res*. **2014**, *47*, 2631−2642.
43. Xue, M.; Yang, Y.; Chi, X.; Zhang, Z.; Huang, F. Pillararenes, a new class of

464 macrocycles for supramolecular chemistry. *Acc. Chem. Res*. **2012**, *45*, 1294–1308.
465 44. Cragg, P.J.; Sharma, K. Pillar[5]arenes: fascinating cyclophanes with a bright
466 future. *Chem. Soc. Rev*. **2012**, *41*, 597–607.
467 45. Yu, G.C.; Jie, K.C.; Huang, F. H. Supramolecular amphiphiles based on host–
468 guest molecular recognition motifs. *Chem. Rev*. **2015**, *115*, 7240–7303.
469 46. Shao, L.; Sun, J.F.; Hua, B.; Huang, F.H. An AIEE fluorescent supramolecular
470 cross-linked polymer network based on pillar[5]arene host–guest recognition:
471 construction and application in explosive detection. *Chem. Commun*. **2018**, *54*,
472 4866–4869.
473 47. Guo, Y.; Guo, S.; Ren, J.; Zhai, Y.; Dong, S.; Wang, E. Cyclodextrin
474 functionalized graphene nanosheets with high supramolecular recognition
475 capability: synthesis and host−guest inclusion for enhanced electrochemical
476 performance. *ACS Nano* **2010**, *4*, 4001–4010.
477 48. Zhu, G.B.; Zhang, X.; Gai, P.B.; Zhang, X.H.; Chen, J.H. β-Cyclodextrin
478 non-covalently functionalized single-walled carbon nanotubes bridged by
479 3,4,9,10-perylene tetracarboxylic acid for ultrasensitive electrochemical sensing of
480 9-anthracenecarboxylic acid. *Nanoscale* **2012**, *4*, 5703–5709.
481 49. Zhou, J.; Chen, M.; Diao, G.W. Calix[4,6,8]arenesulfonates functionalized
482 reduced graphene oxide with high supramolecular recognition capability:
483 fabrication and application for enhanced host–guest electrochemical recognition.
484 *ACS Appl. Mater. Interfaces* **2013**, *5*, 828–836.
485 50. Mao, X.W.; Liu, T.; Bi, J.H.; Luo, L.; Tian, D.M.; Li, H.B. The synthesis of
486 pillar[5]arene functionalized graphene as a fluorescent probe for paraquat in living
487 cells and mice. *Chem. Commun*. **2016**, *52*, 4385–4388.
488 51. Allen, M.J.; Tung, V.C.; Kaner, R.B. Honeycomb carbon: a review of graphene.
489 *Chem. Rev*. **2010**, *110*, 132–145.
490 52. Chen, W.; Zhang, Y.Y.; Li, J.; Lou, X.B.; Yu, Y.H.; Jia, X.H.; Li, C.J. Synthesis of
491 a cationic water-soluble pillar[6]arene and its effective complexation towards
492 naphthalenesulfonate guests. *Chem. Commun*. **2013**, *49*, 7956–7958.
493 53. Yu, G.C.; Zhou, J.; Shen, J.; Tang, G.P.; Huang, F.H. Cationic pillar[6]arene/ATP
494 host–guest recognition: selectivity, inhibition of ATP hydrolysis, and application
495 in multidrug resistance treatment. *Chem. Sci*. **2016**, *7*, 4073–4078.
496 54. Wu, J.R.; Mu, A.; Li, B.; Wang, C.Y.; Fang, L.; Yang, Y.W. Desymmetrized
497 Leaning Pillar[6]arene. *Angew. Chem*. **2018**, *130*, 1–7.

55. Zhao, G.F.; Yang, L.; Wu, S.L.; Zhao, H.; Tang, E.; Li, C.P. The synthesis of amphiphilic pillar[5]arene functionalized reduced graphene oxide and its application as novel fluorescence sensing platform for the determination of acetaminophen. *Biosens. Bioelectron*. **2017**, *91*, 863–869.

56. Zhou, J.; Chen, M.; Xie, J.; Diao, G.W. Synergistically enhanced electrochemical response of host–guest recognition based on ternary nanocomposites: reduced graphene oxide-amphiphilic pillar[5]arene-gold nanoparticles. *ACS Appl. Mater. Interfaces* **2013**, *5*, 11218–11224.

57. Mao, X.W.; Tian, D.M.; Li, H.B. p-Sulfonated calix[6]arene modified graphene as a 'turn on' fluorescent probe for L-carnitine in living cells. *Chem. Commun*. **2012**, *48*, 4851–4853.

58. Liu, Z.; Robinson, J.T.; Sun, X.M.; Dai, H.J. PEGylated nanographene oxide for delivery of water-Insoluble cancer drugs. *J. Am. Chem. Soc*. **2008**, *130*, 10876–10877.

59. Robinson, J.T.; Tabakman, S.M.; Liang, Y.Y.; Wang, H.L.; Casalongue, H.S.; Vinh, D.; Dai, H.J. Ultrasmall reduced graphene oxide with high near-infrared absorbance for photothermal therapy. *J. Am. Chem. Soc*. **2011**, *133*, 6825–6831.

60. Sun, X.M.; Liu, Z.; Welsher, K.; Robinson, J.T.; Goodwin, A.; Zaric, S.; Dai, H.J. Nano-graphene oxide for cellular imaging and drug delivery. *Nano Res*. **2008**, *1*, 203–212.

61. Yang, L.; Zhao, H.; Li, Y.C.; Ran, X.; Deng, G.G.; Zhang, Y.Q.; Ye, H.Z.; Zhao, G.F.; Li, C.P. Indicator displacement assay for cholesterol electrochemical sensing using a calix[6]arene functionalized graphene-modified electrode. *Analyst* **2016**, *141*, 270–278.

62. Fu, G.; Tao, L.; Zhang, M.; Chen, Y.; Tang, Y.; Lin, J.; Lu, T. One-pot, water-based and high-yield synthesis of tetrahedral palladium nanocrystal decorated grapheme. *Nanoscale* **2013**, *5*, 8007–8014.

63. Zhao, H.; Yang, L.; Li, Y.C.; Ran, X.; Ye, H.Z.; Zhao, G.F.; Zhang, Y.Q.; Li, F.; Li, C.P. A comparison study of macrocyclic hosts functionalized reduced graphene oxide for electrochemical recognition of tadalafil. *Biosens. Bioelectron*. **2017**, *89*, 361–369.

64. Zhou, J.; Chen, M.; Diao, G. W. Assembling gold and platinum nanoparticles on resorcinarene modified graphene and their electrochemical applications. *J. Mater. Chem. A* **2013**, *1*, 2278–2285.

65. Ogoshi, T.; Takashima, S.; Yamagishi, T. A. Molecular recognition with microporous multilayer films prepared by layer-by-layer assembly of pillar[5]arenes. *J. Am. Chem. Soc*. **2015**, *137*, 10962−10964.

66. Ogoshi, T.; Yamagishi, T.A.; Nakamoto, Y. Pillar-shaped macrocyclic hosts pillar[n]arenes: new key players for supramolecular chemistry. *Chem. Rev*. **2016**, *116*, 7937–8002.

67. Yao, Y.; Xue, M.; Chen, J.; Zhang, M.; Huang, F. An amphiphilic pillar[5]arene: synthesis, controllable self-assembly in water, and application in calcein release and TNT adsorption. *J. Am. Chem. Soc*. **2012**, *134*, 15712−15715.

68. Hua, B.; Zhang, Z.H.; Sun, J.F.; Yang, J. Pillar[6]arene/acridine orange host–guest complexes as colorimetric and fluorescence sensors for choline compounds and further application in monitoring enzymatic reactions. *Sens. Actuators B* **2018**, *255*, 1430–1435.